

## Quantum paramagnetic fluctuations in $\text{RbFeCl}_3$ in a magnetic field applied perpendicular to the anisotropy axis

B. P. Toperverg

*Institut Laue-Langevin, B.P. 156, F-38042 Grenoble Cedex 9, France  
and Petersburg Nuclear Physics Institute, Gatchina, 188350 St. Petersburg, Russia*

B. Dorner

*Institut Laue-Langevin, B.P. 156, F-38042 Grenoble Cedex 9, France*

A. Sonntag

*Institut Laue-Langevin, B.P. 156, F-38042 Grenoble Cedex 9, France  
and Institut für Experimental Physik, Universität Regensburg, Germany*

D. Petitgrand

*Laboratoire Léon Brillouin-CEN-Saclay, F-91191 Gif-sur-Yvette Cedex, France*

(Received 12 January 1996; revised manuscript received 25 July 1996)

The results for experimental and theoretical studies of the spin dynamics in the crystal of  $\text{RbFeCl}_3$  in a magnetic field up to 5.5 T applied perpendicular to the anisotropy axis are reported. The data for the excitation spectrum collected in the inelastic neutron-scattering experiment at 5.5 K, i.e., well above the phase-transition temperature, are treated in accordance with the theory developed for the quantum paramagnetic fluctuations in spin-1 systems with strong easy-plane-type anisotropy. In order to check the theory, the parameters extracted from the spectrum evaluation are used to calculate the expected dependencies of the ratios between intensities of two measured excitation branches on momentum transfer and magnetic field. No additional fitting parameters are needed to obtain a satisfactory agreement with the experimental ratios. [S0163-1829(97)06701-5]

### I. INTRODUCTION

The  $\text{Fe}^{2+}$  ion in the family of ternary compounds  $A\text{FeX}_3$  (with  $A = \text{Rb}$  or  $\text{Cs}$  and  $X = \text{Cl}$  or  $\text{Br}$ ) has an effective spin  $S = 1$ . A single-site anisotropy caused by the interaction with the crystal field leads locally to a splitting of the triplet state into a singlet ( $m = 0$ ) ground state and a doublet of excited states with  $m = \pm 1$ . These compounds have at room temperature the same hexagonal structure with space group  $P6_3/\text{mmc}$ .<sup>1</sup> Chains of phase sharing  $\text{FeX}_6$  octahedra along the  $c$  axis are separated by the  $A$  ions. The exchange interaction between the chains is antiferromagnetic in all four compounds, while in the Cl compounds the Fe ions are coupled ferromagnetically along the chains and antiferromagnetically in the Br compounds. The magnetic interaction along the chains is about ten times stronger than between them. This leads to quasi-one-dimensional features of the excitation spectrum. In all compounds the uniaxial easy-plane anisotropy is rather strong and, for example, in the Cs compounds it is so strong that the whole crystal remains in a singlet ground state (SGS) for  $T \rightarrow 0$ . SGS's are also of interest in context with the study of the Haldane gap for  $S = 1$  one-dimensional Heisenberg antiferromagnets.<sup>2</sup>

The Rb compounds exhibit long-range order at low temperature. In  $\text{RbFeCl}_3$ ,<sup>3,4</sup> two incommensurate magnetic structures appearing at 2.50 and 2.35 K are followed below 1.95 K by a commensurate phase found with ferromagnetic order along the chains and the frustrated  $120^\circ$  structure in the hexagonal plane. The excitations and the soft mode behavior in this phase were studied by neutron scattering in Refs. 5–7.

A magnetic field  $H_{\parallel}$  applied parallel to the hexagonal axis ( $c$  axis) in  $\text{CsFeCl}_3$  (Refs. 8–10) and  $\text{CsFeBr}_3$  (Ref. 11) leads at low temperature to a linear Zeeman splitting of the excited doublet. Long-range order appears in  $\text{CsFeCl}_3$  at  $T = 0.7$  K,  $H_{\parallel} = 3.8$  T (incommensurate) and  $T = 0.7$  K,  $H_{\parallel} = 4.5$  T (commensurate), while in  $\text{CsFeBr}_3$  the order becomes directly commensurate at  $T = 1.6$  K,  $H_{\parallel} = 4.1$  T. The influence of the magnetic field applied perpendicular to the anisotropy axis on the magnetic excitations depends on the character of the exchange interaction along the chains. In  $\text{CsFeBr}_3$ , with antiferromagnetic coupling along the chains, the frequencies and intensities of the excitations were found to be independent of the applied field up to 6 T.<sup>12</sup> In  $\text{CsFeCl}_3$ , however, both the frequencies and intensities were dramatically influenced by the field.<sup>13</sup> The frequencies were interpreted following a theoretical approach by Lindgård and Schmid.<sup>14</sup> The agreement was reasonable, with discrepancies between experiment and theory at the higher frequencies of the spectrum at high fields. There was no satisfactory theoretical prediction available on the wave vector and field dependence of intensities.

In the following we present an investigation of  $\text{RbFeCl}_3$ , in which the exchange interaction along the chains is also ferromagnetic, in an external field applied perpendicular to the anisotropy axis. Section II presents a theoretical derivation of explicit expressions, which are used for a description of both frequencies and intensities in dependence on the field, and results of other theoretical approaches are briefly commented upon. In Sec. III we describe the experiment, and present the experimental results. A discussion and comparison with theory follows in Sec. IV.

## II. THEORY

### A. General

The problems related to spin dynamics in strongly anisotropic spin-1 systems have been under extensive theoretical discussion for a long time, and a number of rather interesting results have been obtained in this field using different theoretical methods including the random-phase approximation,<sup>10</sup> the correlated-effective-field<sup>15</sup> and dynamical correlated-effective-field approximations,<sup>16,17</sup> the  $1/n$  and strong-coupling limit expansion,<sup>18</sup> the correlation theory approach based on the Mori formalism (see Ref. 14, and references therein), etc.

However, most of the theoretical results were formulated in a such way that the approximations used in the derivation are hardly to be controlled, while the final equations are represented in a form which makes it difficult to apply them immediately for the description of our experiment. Therefore, aiming at practical use, here we present a simple derivation of the explicit equations for the components of the nonuniform dynamic susceptibilities directly related to the intensities of magnetic inelastic neutron scattering.

We shall use the quantum field theory formulation of the perturbation theory developed for spin operators by Vaks, Lakin, and Pikin (VLP) a long time ago.<sup>19,20</sup> In Ref. 20 this theory was applied for calculations of the fluctuational renormalization of the spin wave (SW) parameters in Heisenberg ferromagnets, while in Ref. 21 to those in anisotropic antiferromagnets. Recently it was used to treat the problem of dipolar dynamics<sup>22</sup> in ferromagnets.

For us it is important that VLP theory predicts a general structure of the response function in the case of developed fluctuations, and that even in this case the propagating modes of the excitations may still survive in a certain range of wave vectors. In the present experiment the data were mostly collected in a range of parameters, i.e., wave vectors and frequencies of the excitations, and temperatures and magnetic fields in which no appreciable line broadening of the inelastic scattering signal could be detected. This experimental evidence is actually used as an argument in favor of the approach employed below.

The standard parametrically defined perturbation VLP diagrammatic expansion formulates as a first step a regular procedure to develop propagating modes starting from single-site excitations. This is especially convenient in our case because of the strong single-site anisotropy, which invokes to use these excitations as reference ones.<sup>14–17</sup>

### B. Hamiltonian

The effective-spin Hamiltonian of the system derived by Eibschütz, Lines, and Sherwood<sup>15</sup> may be represented as a sum of two terms,

$$\mathcal{H} = \mathcal{H}_0 + \mathcal{H}_{\text{int}}. \quad (1)$$

The reference Hamiltonian  $\mathcal{H}_0$  corresponds to the noninteracting spins  $\mathbf{S}_i$  situated at sites  $i$  affected by the strong single-ion anisotropy and the effective magnetic field  $\mathbf{H}$ ,

$$\mathcal{H}_0 = \sum_i \mathcal{H}_{0i} = \sum_i \{D(S_i^z)^2 - \mu \mathbf{H}_i \mathbf{S}_i\}, \quad (2)$$

where  $D$  is the anisotropy constant (or, in accordance with Ref. 15, the zero-field splitting parameter),  $\mu = g \mu_B$  is the magnetic moment of the  $\text{Fe}^{2+}$  ion, and  $\mu_B$  is the Bohr magneton. For simplicity here we have written a  $g$  factor, while in anisotropic systems one should, strictly speaking, use a tensor  $\hat{g}$ , which, in accordance with Ref. 15, has two independent components  $g_{\parallel}$  and  $g_{\perp}$  (see also Ref. 23). In our field configuration we denote  $g = g_{\perp}$  in Eq. (2), and small orthorhombic distortions<sup>15</sup> are neglected.

The effective on-site field  $\mathbf{H}_i$  is a sum of two terms:  $\mathbf{H}_i = \mathbf{H}_e + \sum_j J_{ij} \mathbf{m}_j / \mu$ , and for an homogeneous system it is independent of the site, i.e.,  $\mathbf{H}_i = \mathbf{H}$ . In this sum  $\mathbf{H}_e$  is the external magnetic field, and the second term corresponds to the molecular field created by the average on-site magnetization  $\mu \mathbf{m}$ , where

$$\mathbf{m} = \mathbf{m}_i = \langle \mathbf{S}_i \rangle = \text{Tr}\{e^{-\mathcal{H}_i/T} \mathbf{S}_i\} / \text{Tr}\{e^{-\mathcal{H}_i/T}\}, \quad (3)$$

via exchange interaction.

Since we have introduced the effective field, then the second term in Eq. (1) describes the exchange interaction between the spin fluctuations,

$$\mathcal{H}_{\text{int}} = -\frac{1}{2} \sum_{i \neq j} J_{ij} (\mathbf{S}_i - \mathbf{m})(\mathbf{S}_j - \mathbf{m}). \quad (4)$$

The Fourier transform  $J_{\mathbf{q}}$  of the exchange integral  $J_{ij}$  may be approximated as follows:<sup>11</sup>

$$J_{\mathbf{q}} = 4\{[J_1 \cos q_z + J_2 \cos 2q_z] + J' \gamma(q_x, q_y)\}, \quad (5)$$

where  $\gamma(q_x, q_y) = 2 \cos q_y \{\cos q_x + \cos q_x\} - 1$ , and  $q_z$  is the wave-vector component along the  $c$  axis, while  $q_x$  and  $q_y$  are displayed in the basal plane. The constant of the ferromagnetic exchange  $J_1 > 0$  between the nearest neighbors along the chains is about one order of magnitude larger than the antiferromagnetic exchange integral  $J_2 < 0$  between the next-nearest neighbors within the chains, as well as the constant  $J' < 0$  of the antiferromagnetic coupling between the chains (see Refs. 1 and 15).

On the other hand, the anisotropy constant  $D$  is about one order of magnitude greater than  $J_1$ —the largest of the exchange constants.<sup>1,5,15</sup> Thus within a broad range of the wave vectors  $2J_{\mathbf{q}} \ll D$ , and only in the vicinity of points with coordinates in the reciprocal space,  $q_z^{\text{max}} = 0$ ,  $q_x^{\text{max}} = 0$ , and  $q_y^{\text{max}} = 2\pi/3$ ,  $4\pi/3$  (or  $q_x^{\text{max}} = \pi$  and  $q_y^{\text{max}} = \pi/3, 5\pi/3$ ), is the energy of the exchange interaction comparable with the anisotropy, i.e.,  $2J_{\mathbf{q}^{\text{max}}} \sim D$ .

Therefore we shall consider the exchange coupling as a perturbation with respect to the anisotropy—the leading interaction in the system. As we shall see, this idea appears to be quite fruitful in a description of the collective excitations around  $\mathbf{q} \sim \mathbf{q}^{\text{max}}$ . In this range of wave vectors the spectrum varies strongly with the temperature if  $T \leq \{D - 2J_{\mathbf{q}^{\text{max}}}\}$ . Its softening may finally lead to the phase transition instability at  $T = T_N$ .

### C. Single site excitations

Apart from the range of  $\mathbf{q} \sim \mathbf{q}^{\text{max}}$  the spectrum is mostly defined by the single-site spin excitations given by the zero-order Hamiltonian  $\mathcal{H}_0$ . For  $\mathbf{H}_e = 0$  the spectrum of this Hamiltonian has two stationary states: a nondegenerated

ground state ( $E_0=0$ ) and a degenerated doublet with  $E_{1,2}=D$ . Correspondingly, the spectrum of the single-site excitation is characterized by only one energy,  $E_{1,2}-E_0=D$ . An applied magnetic field  $\mathbf{H}_e$  lifts the degeneracy of the doublet. If the field is directed along the anisotropy axis, i.e.,  $H_e=H_z$ , then the operator  $S^z$  has a set of the eigenvectors in common with the Hamiltonian  $\mathcal{H}_0$ , and the stationary states may be characterized by the set of the eigenvalues  $m^z=-1, 0$ , and  $1$  of the  $S^z$  operator. In each of these states the expectation values  $\langle S^{x(y)} \rangle = m^{x(y)} = 0$ , while  $\langle \mathbf{S}^2 \rangle = S(S+1) = 2$ . This means that in any stationary state each of the projections  $m^\alpha$  of the vector  $\mathbf{m}$  experiences rather extensive quantum fluctuations characterized by the mean-square deviations  $\delta(m^\alpha)^2 = \langle (S^\alpha)^2 \rangle - \langle S^\alpha \rangle^2$ , and by the correlation tensor  $\langle S^\alpha S^\beta \rangle$ .

If the magnetic field  $H_e=H_x$  is applied along the  $x$  axis, i.e., perpendicular to the anisotropy axis, the spectrum of the Hamiltonian contains three nondegenerated energy levels: the ground-state term with  $E_0=1/2(D-\Delta)$  and two excited states with  $E_1=D$  and  $E_2=1/2(D+\Delta)$ , respectively, where  $\Delta=[D^2+4\mu^2H_e^2]^{1/2}$ . None of the single-site spin projections commute with the Hamiltonian  $\mathcal{H}_0$  and, thus, they are no longer conserved quantities in any of the stationary states of the Hamiltonian  $\mathcal{H}_0$ . This means that all projections of the local magnetization experience rather developed quantum fluctuations in each of the stationary states.

On the basis of the Hamiltonian eigenfunctions the symmetrical  $3 \times 3$  matrix of the  $S^z$  operator contains only four nonzero elements:  $S_{01}^z = S_{10}^z = -(\varepsilon_{21}/\Delta)^{1/2}$  and  $S_{21}^z = S_{12}^z = (\varepsilon_{10}/\Delta)^{1/2}$ , which describe the transitions between the corresponding stationary states with the energies of single-site excitations:  $\varepsilon_{20}=E_2-E_0=\Delta$ ,  $\varepsilon_{21}=E_2-E_1=-E_0$ , and  $\varepsilon_{10}=E_1-E_0=E_2$ . The nonzero elements of the antisymmetrical matrix of the operator  $S^y$  are related to the elements of  $S^z$  in the following way:  $S_{01}^y = -S_{10}^y = -iS_{21}^z$  and  $S_{21}^y = -S_{12}^y = iS_{01}^z$ . Only the matrix of the operator  $S^x$  has two diagonal elements  $S_{00}^x = -S_{22}^x = 2\mu H/\Delta$ , which corresponds to the nonzero expectation values for the magnetization projections onto the magnetic-field direction. However, this matrix is nondiagonal and also contains two elements:  $S_{02}^x = S_{20}^x = -D/\Delta$ .

Having these explicit equations for the spin projection matrix elements one can easily analyze the correlations between the fluctuations of different projections of the local magnetization. They are generally characterized by the retarded Green function, which is defined as a mean value of the commutator  $G_{ij}^{\alpha\beta}(t) = -i\langle \{S^\alpha(t) - m_i, S^\beta(0) - m_j\} \rangle$  at  $t > 0$ , and  $G^{\alpha\beta}(t) = 0$  at  $t < 0$ . Its Fourier transform

$$G_{\mathbf{q}}^{\alpha\beta}(\omega) = \frac{1}{N} \sum_{ij} e^{i\mathbf{q}(\mathbf{r}_i - \mathbf{r}_j)} \int dt e^{-i\omega t} G_{ij}^{\alpha\beta}(t) \quad (6)$$

is, as is well known (see Refs. 24–26), proportional to the tensor of the nonuniform dynamic magnetic susceptibility describing the reaction of the system on the alternating magnetic field:

$$\chi_{\mathbf{q}}^{\alpha\beta}(\omega) = \frac{\omega_0}{4\pi} G_{\mathbf{q}}^{\alpha\beta}(\omega), \quad (7)$$

where  $\omega_0 = 4\pi\mu^2/v_0$ , and  $v_0$  is the volume per one atomic spin.

On the other hand, at  $\omega \neq 0$  the imaginary part of the Green function is expressed via the Fourier transform of the pair spin-correlation function,

$$\langle S_{\mathbf{q},\omega}^\alpha S_{-\mathbf{q},-\omega}^\beta \rangle = 2[N(\omega) + 1] \text{Im} G_{\mathbf{q}}^{\alpha\beta}(\omega), \quad (8)$$

where  $N(\omega) = [\exp(\omega/T) - 1]^{-1}$ . This function is related to the inelastic neutron-scattering cross section (see below) measured in the experiment.

The invariant form of the perturbation theory is formulated not for the retarded, but for the temperature Green function.<sup>24</sup> Therefore, following the standard procedure (see, for example, Refs. 24 and 19–22), we first calculate the latter function and then the retarded Green function, as an analytic continuation of the temperature Green function  $G_{\mathbf{q}}^{\alpha\beta}(i\omega_n)$  from the discrete sequence of the imaginary Matsubara frequencies  $i\omega_n = 2\pi nT$  (with  $n > 0$  an integer number) onto the real axis of  $\omega$ . Following this procedure and using the matrix elements of the spin operators given above, one immediately obtains the following set of equations for the single-site Green functions  $G_{ij}^{\alpha\beta}(\omega) = \sum_0^{\alpha\beta}(\omega) \delta_{ij}$ :

$$\Sigma_0^{xx}(\omega) = \frac{2}{\Delta} \rho_{20} \frac{D^2}{\omega^2 - \Delta^2}, \quad (9)$$

$$\Sigma_0^{yy}(\omega) = \frac{2}{\Delta} \left\{ \rho_{10} \frac{\varepsilon_{10}^2}{\omega^2 - \varepsilon_{10}^2} + \rho_{21} \frac{\varepsilon_{12}^2}{\omega^2 - \varepsilon_{12}^2} \right\}, \quad (10)$$

$$\Sigma_0^{zz}(\omega) = \frac{2}{\Delta} \left\{ \rho_{10} \frac{\varepsilon_{10}\varepsilon_{12}}{\omega^2 - \varepsilon_{10}^2} - \rho_{12} \frac{\varepsilon_{10}\varepsilon_{12}}{\omega^2 - \varepsilon_{12}^2} \right\}, \quad (11)$$

$$\Sigma_0^{yz} = -\Sigma_0^{zy} = -\frac{2i}{\Delta} \left\{ \rho_{10} \frac{\mu H \omega}{\omega^2 - \varepsilon_{10}^2} + \rho_{12} \frac{\mu H \omega}{\omega^2 - \varepsilon_{12}^2} \right\}, \quad (12)$$

where  $\rho_{\lambda\lambda'} = \rho_\lambda - \rho_{\lambda'}$ , and  $\rho_\lambda = \exp(-E_\lambda/T) / \sum_\lambda \exp(-E_\lambda/T)$  are the statistical weights of the corresponding eigenstates  $\lambda = 0, 1$ , and  $2$  of the Hamiltonian  $\mathcal{H}_0$ , and  $H = H(m^x)$  is defined by the mean-field equation  $m^x = (2\mu H/\Delta) \{ \rho_{02} \}$ .

We see that the tensor of the single-site spin correlations  $\sum_0^{\alpha\beta}(\omega)$  has only four different nontrivial components corresponding to the different polarizations of the spin projection fluctuations. One of these modes of fluctuations is linearly polarized along the field, and has the characteristic frequency  $\varepsilon_{20} = E_2 - E_0 = \Delta$  which corresponds to the virtual transition between the ground and the highest-energy level. Three other components describe a kind of superposition of the two frequency elliptic precession of the spin projections in the plane perpendicular to the field. The ellipticity is apparently a consequence of the uniaxial anisotropy in this plane. One of these two frequencies  $\varepsilon_{10} = E_1 - E_0 = 1/2(D + \Delta)$  corresponds to the virtual transition from the ground to the first excited state, while another one reflects the contribution to the precession coming from the virtual transition between two excited states, i.e.,  $\varepsilon_{12} = E_1 - E_2 = 1/2(D - \Delta)$ . As long as the interspin interaction is switched off, the phases of precession (or relevant events of the virtual transitions) randomly change from site to site, but the exchange interaction brings them into coherence.

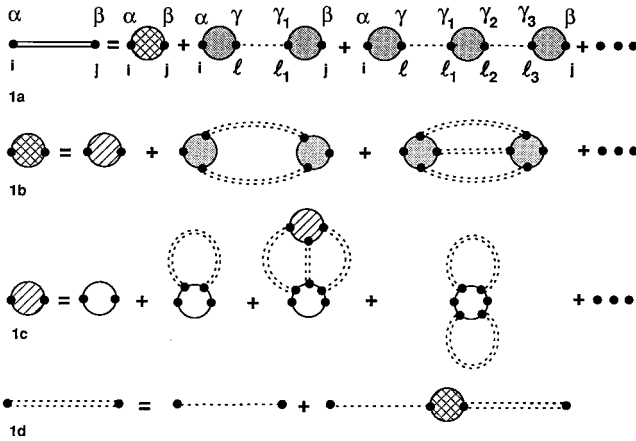


FIG. 1. Sketch of the diagrammatic representation of the VLP perturbation theory series expansion.

Equations (9)–(12), which are just intermediate results, appear quite similar to those obtained in Ref. 16 for the ordered phase in the field equal to zero. This is simply due to the fact that the single-site Hamiltonian has the same structure, containing two terms: linear and quadratic ones with respect to the spin projection operators. However, the parameters of the Hamiltonian are different, as well as an exact form of corresponding equations for the single-site Green functions. In particular, in Ref. 16 the anisotropy constant is partly renormalized by use of a correlation parameter introduced into the single-site Hamiltonian. This parameter and the single-site staggered magnetization are then defined by a pair of equations: one follows from the condition of self-consistency [similar to that in the mean-field approximation (MFA)], and the other one from the fluctuation dissipation theorem. In our case, we have the field-induced magnetization directed perpendicular to the anisotropy axis. Due to symmetry reasons we cannot describe this case by only homogeneous renormalization, characterized by a unique correlation parameter.<sup>16</sup> Therefore here we discuss an alternative way of renormalization.

#### D. Interspins interaction as a perturbation. Larkin equation

The physical picture behind the perturbation theory approach is as follows. Each event of the virtual change of a spin state at a given site distorts the local molecular field on the neighboring spins. This may provoke changes in their states, which creates the fluctuational molecular field on the next neighbors, and so on, providing a mechanism for the collectivization of single-site excitations and, in particular, spin-wave propagation. This is illustrated in Fig. 1(a), where cross-hatched circles denote the total irreducible blocks  $\Sigma_{ij}^{\alpha\beta}(i\omega_n)$  linked into the chain via dashed lines corresponding to the interspin interaction  $J_{ij}$ , and the double solid line describes the collective-mode propagation between sites  $i$  and  $j$ .

The diagrammatic expansion in Fig. 1(a) directly follows from the definition of the temperature Green function  $G_{ij}^{\alpha\beta}(i\omega_n)$  if one expands the evolution operator  $\sigma(1/T)$  (Refs. 19–22) into a power series with respect to the inter-

action Hamiltonian  $\mathcal{H}_{\text{int}}$  and, averaging the products of the spin projection operators, takes into account the fact that  $J_{ij}=0$  at  $i=j$ .

Thus in Fig. 1 crossed-hatched circles with two points on a circle correspond to the average of the products of couples of spin projection operators, which may belong to the same site, while dashed lines connect the sites with  $l \neq l_1, l_2 \neq l_3$ , etc. These products can be decomposed into a sum of terms, as shown in Fig. 1(b), where the hatched circle denotes the total single-site block  $\Sigma^{\alpha\beta}(i\omega_n)$ , which corresponds to the average of a pair of spin projection operators at the same site. The diagrams for this block are given in Fig. 1(c). Other terms in Fig. 1(b) correspond to the case when spins belong to different sites. These terms contain irreducible blocks of higher orders (three-spin, four-spin, etc. Green functions) shown as hatched circles with more than two points on each. They are connected by the dashed double lines, which correspond to the effective dynamical interspin interaction  $V_{ij}^{\alpha\beta}(i\omega_n)$ . This may be represented via exchange interaction and the total irreducible blocks, as shown in Fig. 1(d) and, in accordance with Fig. 1(a), via the Green function  $G_{ij}^{\alpha\beta}(i\omega_n)$ .

The first diagram in Fig. 1(c) shown by an open circle with two points on it corresponds to the mean-field single-site susceptibility  $\Sigma_0^{\alpha\beta}(i\omega)$  given in Eqs. (9)–(12). The other diagrams shown in Fig. 1(c) describe the single-site susceptibility renormalization due to the creation of the virtual collective excitations in the spin medium.

Similar renormalization should also be applied to the local spin average  $\langle S^x \rangle$ . The process of such a renormalization may be illustrated in the same way as in Fig. 1(c), in which the hatched circle with two points should be substituted for by a circle with one point on it, and the number of points on each circle in Fig. 1(c) should be reduced by one. Thus an open circle with one point on it will correspond to  $\langle S^x \rangle$  in the MFA, while the second diagram shows the same quantity renormalized due to the creation and absorption of a fluctuation. Also, one may consider the processes of creation of more than one collective mode by the local excitation and the exchange between spins by several (virtual) modes, as shown in Fig. 1(c). The circles containing more than two points correspond to the amplitudes of a decay of the spin fluctuations into several ones, or to their scattering by each other. Of course, they may be “dressed” by the fluctuating fields and “delocalized,” as shown in Fig. 1(b).

Resolving the series of diagrams given in Fig. 1(a), one immediately obtains the set of Larkin equations,

$$G_{\mathbf{q}}^{\alpha\beta}(i\omega_n) = \Sigma_{\mathbf{q}}^{\alpha\beta}(i\omega_n) + \sum_{\gamma=xyz} \Sigma_{\mathbf{q}}^{\alpha\gamma}(i\omega_n) J_{\mathbf{q}} G_{\mathbf{q}}^{\gamma\beta}(i\omega_n). \quad (13)$$

As follows from Eqs. (9)–(12), this set contains four equations, and only three of them are interconnected, while the solution of the separated equation for the longitudinal (i.e., parallel to the field) component of the tensor  $G_{\mathbf{q}}^{\alpha\beta}(i\omega_n)$  is written as

$$G_{\mathbf{q}}^{xx}(i\omega_n) = \frac{\Sigma_{\mathbf{q}}^{xx}(i\omega_n)}{1 - J_{\mathbf{q}} \Sigma_{\mathbf{q}}^{xx}(i\omega)}. \quad (14)$$

Solving the three equations for the other nonzero components of the tensor, one has

$$G_{\mathbf{q}}^{yy(zz)}(i\omega_n) = \{1 - J_{\mathbf{q}} \sum_{\mathbf{q}'}^{zz(yy)}(i\omega_n) - R_{\mathbf{q}}(i\omega_n)\} / J_{\mathbf{q}} R_{\mathbf{q}}(i\omega_n), \quad (15)$$

$$G_{\mathbf{q}}^{yz(zy)}(i\omega_n) = \sum_{\mathbf{q}'}^{yz(zy)}(i\omega_n) / R_{\mathbf{q}}(i\omega_n), \quad (16)$$

$$R_{\mathbf{q}}(i\omega_n) = 1 - J_{\mathbf{q}} [\sum_{\mathbf{q}'}^{zz}(i\omega_n) + \sum_{\mathbf{q}'}^{yy}(i\omega_n)] + J_{\mathbf{q}}^2 [\sum_{\mathbf{q}'}^{zz}(i\omega_n) \sum_{\mathbf{q}'}^{yy}(i\omega_n) - \sum_{\mathbf{q}'}^{zy}(i\omega_n) \sum_{\mathbf{q}'}^{yz}(i\omega_n)], \quad (17)$$

where the excitation spectrum is defined by the solutions of the equation  $R_{\mathbf{q}}(\omega) = 0$ .

From these equations we see not only how interaction develops the discrete single-site spectrum into continuous branches of collective modes, but also that the modes of excitations with the polarization vectors displayed within the plane perpendicular to the magnetic field are built up from all single-site modes with polarizations in this plane.

### E. Spin waves in the mean-field approximation

To elucidate the situation, let us consider the first order of the perturbation theory and, thus, set  $\sum_{\mathbf{q}}^{\alpha\beta}(\omega) \approx \sum_0^{\alpha\beta}(\omega)$  defined by Eqs. (9)–(12). Also, we assume that the temperature  $T \ll D$  and the two upper levels of the single-site spectrum are almost unpopulated, i.e., that in Eqs. (9)–(12)  $\rho_{10} \approx \rho_{20} \approx -1$ , while  $\rho_{21} \approx 0$ . Then, from Eq. (14), it follows that

$$G_{\mathbf{q}}^{xx}(\omega) = -\frac{2}{\Delta} \frac{D^2}{\omega^2 - \Omega_{1\mathbf{q}}^2}, \quad (18)$$

where the spectrum of this mode of the excitations is defined as follows:

$$\Omega_{1\mathbf{q}}^2 = \Delta^2 - 2D^2(J_{\mathbf{q}}/\Delta). \quad (19)$$

From Eqs. (18) and (19) it is clearly seen how the exchange interaction brings a dispersion into the spectrum, and how, at elevated fields, it goes away from the instability related to the point of compensation of the anisotropy by the exchange at  $\mathbf{q}^{\max}$ . The magnetic field increases the energy of spin fluctuations, and decreases the weight of the exchange-interaction contribution into this branch of the spectrum. This makes the dispersion curve more flat.

The Green function for all types of fluctuations of the spin projections may be written in the general form

$$G_{\mathbf{q}}^{\mu\nu}(\omega) = \frac{\Lambda^{\mu\nu}}{\omega^2 - \Omega_{i\mathbf{q}}^2}, \quad (20)$$

where  $\mu, \nu = x, y, z$ . The amplitude  $\Lambda^{xx} = -2D^2/\Delta$  and for  $i=1$  the frequency  $\Omega_{1\mathbf{q}}$  is given by Eq. (19), while amplitudes of the fluctuations of the spin projections perpendicular to the field are defined as follows:

$$\Lambda^{yy} = -\frac{1}{\Delta} \{2\varepsilon_{10}\Delta - (2\mu H)^2[\frac{1}{2} + (J_{\mathbf{q}}/\Delta)]\}, \quad (21)$$

$$\Lambda^{zz} = \frac{1}{\Delta} \{2\varepsilon_{10}[\varepsilon_{10} - \Delta] + (2\mu H)^2(J_{\mathbf{q}}/\Delta)\}, \quad (22)$$

$$\Lambda^{yz} = -\Lambda^{zy} = 2i\omega\mu H/\Delta. \quad (23)$$

For all those fluctuations the spectrum  $\Omega_{i\mathbf{q}} = \Omega_{2\mathbf{q}}$  is unique, and given by the equation

$$\Omega_{2\mathbf{q}}^2 = \varepsilon_{10}^2 - 2J_{\mathbf{q}}\varepsilon_{10} + (2\mu H)^2(J_{\mathbf{q}}/\Delta)^2. \quad (24)$$

At  $H=0$  this equation coincides with Eq. (19), as it should.

In an applied field this degeneracy of  $\Omega_{1\mathbf{q}}$  and  $\Omega_{2\mathbf{q}}$  is lifted, but not for all wave vectors, as it seems at first sight. Indeed, an applied magnetic field increases the energy of excitations for all wave vectors, but it distorts different branches of the excitations in a different way. In particular, the dispersion curve  $\Omega_{2\mathbf{q}}$  for certain directions does become steeper and not flatter. This behavior is related to the  $J_{\mathbf{q}}^2$  term in Eq. (24).

As a consequence, two dispersion surfaces may have a line of intersection in reciprocal space, defined by the equation  $\Omega_{1\mathbf{q}} = \Omega_{2\mathbf{q}}$ . For the wave vectors belonging to this line the fluctuations of the magnetization projections parallel to the magnetic field have the same frequency as fluctuations polarized in the plane perpendicular to the field.

At low fields the line of degeneracy is a solution of the equation

$$J_{\mathbf{q}} \approx D[3 - \sqrt{17}]/4, \quad (25)$$

which is in this approximation independent on the magnetic-field strength. This means that at low fields both types of fluctuations, with the wave vectors defined by this equation, experience the same influence of the magnetic field. However, for the range of  $q$  space at one side of the line given by Eq. (25), the magnetic field suppresses the fluctuations with one polarization more efficiently, while in the range on the other side it is more efficient for another polarization. As we shall see, for our set of parameters Eq. (25) has a solution at the range of the wave vectors where  $J_{\mathbf{q}}$  is close to its minimum. Unfortunately, the resolution of the instrument was not good enough to verify the intersection of those branches. On the other hand, this question is quite interesting from a theoretical point of view. Indeed, Eqs. (19), (24), and (25) are derived in the mean-field approximation and the fluctuational correction may change the conclusion drawn above.

Here it is important to note that the equations above contain an effective magnetic field which is to be found in the same approximation as was used for their derivation. The corresponding transcendental equation for this field  $H$  reads

$$H = H_e + \frac{2J_0 H}{\sqrt{D^2 + (2\mu H)^2}}, \quad (26)$$

where  $J_0$  is the exchange integral at  $\mathbf{q}=0$ . At low effective fields the solution of this equation gives the following linear dependency:  $H(H_e) \approx H_e/(1 - 2J_0/D)$ , which reflects the enhancement of the effective field on a given spin due to the positive exchange interaction, with neighboring spins ‘‘magnetized’’ in an external magnetic field. If the parameter  $1 - 2J_0/D \ll 1$ , then at low external fields the effective field  $H \gg H_e$ .

This solution of Eq. (26) is valid at the applied fields  $2\mu H_e \ll H^* = (D - 2J_0)^{3/2}/2J_0^{1/2}$ . Within the range of external fields  $H^* \ll \mu H_e \ll D/2$  the effective field is approximated by the following equation:  $\mu H \approx (J_0 D \mu H_e)^{1/3}$ . At extremely high fields  $2\mu H_e \gg D$  the effective field  $\mu H \approx \mu H_e + J_0/2$ , i.e., it is still higher than an applied field.

If one defines the energy of the Zeeman splitting as  $E_Z = \mu^{\text{eff}}(H_e)H_e$ , where  $\mu^{\text{eff}} = \tilde{g}(H_e)\mu_B$ , then within the framework of the MFA the effective  $\tilde{g}$  factor should reach its highest value  $\tilde{g} = g/(1 - 2J_0/D)$  at low fields, fall down proportionally to  $H_e^{-2/3}$  within the range  $\mu H^* \ll \mu H_e D/2$  and approach its asymptotic value  $\tilde{g} \approx g$  at highest fields.

One must, however, admit that these conclusions may have quite a restricted range of validity (or even be incorrect) if the difference  $D - 2J_0 \ll D$ . In the particular compound  $\text{RbFeCl}_3$ , as we shall see, it is relatively small. As a result, the correlations of the ferromagnetic type fluctuations are quite developed, which reflects the tendency of the system toward one-dimensional ferromagnetic ordering along the chains. These fluctuations not only bring appreciable corrections to the solutions obtained in the MFA, but, as is well known, they prevent the ordering in low-dimensional systems predicted by the MFA.

Fortunately, in our case the system is not very close to the instability point defined (in the MFA) by the equation  $D = 2J_0$ . Moreover, a relatively weak in-plane antiferromagnetic exchange interaction is sufficient to lead the system away from the instability with respect to the one-dimensional ferromagnetic ordering. Therefore, we believe that fluctuations do not bring drastic changes to the behavior of the system, and their influence may be accounted for by a proper generalization of the results obtained in the MFA. The other important consequence following from the fact that the ferromagnetic susceptibility of the system is quite high should however be discussed separately.

#### F. Demagnetizing effects

The magnetic field inside the sample is defined as

$$H_i^\alpha = H_e^\alpha - 4\pi N^{\alpha\beta} M^\beta. \quad (27)$$

The difference between  $H_e$  and  $H_i$  arises due to the contribution of the induced magnetization  $M^\alpha = \chi^{\alpha\beta} H_e^\beta$ , and depends on the sample shape. This representation of the magnetization is valid for the ellipsoidal sample, and the components of the demagnetization tensor  $N^{\alpha\beta}$  are related to the major axis of the ellipsoid (see Ref. 25).

The susceptibility tensor of a sample  $\chi^{\alpha\beta}(\mathbf{H}_i)$  is generally a function of the internal field  $\mathbf{H}_i$ . It should satisfy the following equation:<sup>26</sup>

$$\chi^{\alpha\beta} = \chi_0^{\alpha\beta} - 4\pi \chi_0^{\alpha\mu} N^{\mu\nu} \chi^{\nu\beta}, \quad (28)$$

where  $\chi_0^{\alpha\beta}(\mathbf{H}_i)$  is the susceptibility of the magnetic matter, while  $\chi^{\alpha\beta}$  is the susceptibility of the sample. In fact, the susceptibility  $\chi_0^{\alpha\beta}$  corresponds to the Green functions considered above, if one substitutes an external magnetic field in these functions with the internal one.

If the magnetic field  $H_e = H_x$  is directed along one of the ellipsoid axes, then the solution of this equation has a simple form,

$$\chi^{xx} = \frac{N^x \chi_0^{xx}}{1 + 4\pi \chi_0^{xx}}, \quad (29)$$

where  $N^x$  is the demagnetization factor in the direction of the applied field, and  $\chi^{xx}$  and  $\chi_0^{xx}$  are the corresponding components of the susceptibilities of the sample and the matter.

Substituting Eq. (29) into Eq. (27) for the internal field then gives the following equation:

$$H_i = \frac{H_e}{1 + 4\pi N^x \chi_0^{xx}(H_i)}. \quad (30)$$

This nonlinear equation cannot be solved analytically for the general case even using the equations for  $\chi_0^{xx}(H_i)$  derived in the MFA. However, an analysis of limiting cases similar to that has been carried out in Refs. 26, 27 and 22; let us draw conclusions on the qualitative behavior of the internal magnetic field as a function of the field applied to a sample. Indeed, from Eq. (30) it follows that if the susceptibility  $\chi_0(H_i)$  is high, then the internal field  $H_i \ll H_e$ , which is a direct consequence of the demagnetization effect. On the other hand, the susceptibility reaches its maximum value at fields equal to zero, and it decreases if an internal field magnetic-field strength increases. As a result, the internal magnetic field may be much smaller than the  $H_e$  at low applied fields, while it approaches  $H_e$  if the applied fields are high enough.

This may readily be demonstrated using the equations obtained above. In the framework of the MFA, the uniform static susceptibility  $\chi_0^{xx} = (\omega_0/4\pi)G^{xx}$ , in accordance with Eq. (18), has the following form:

$$\chi_0^{xx} = \frac{\omega_0}{4\pi} \frac{2D^2}{\Delta^3(H_i) - 2J_0 D^2}, \quad (31)$$

where  $\Delta(H_i) = \sqrt{D^2 + (2\mu H_i)^2}$ . This equation should be substituted into Eq. (30), and solved with respect to  $H_i$ .

At low values of  $H_e$ , the susceptibility  $\chi_0^{xx} \approx 2\omega_0/\{4\pi(D - 2J_0)\}$ , and

$$\mu H_i \approx (D - 2J_0) \frac{\mu H_e}{\Delta_0} \left\{ 1 + \frac{3\mu H_e}{2\Delta_0} + \dots \right\}, \quad (32)$$

where  $\Delta_0 = \{D - 2J_0 + 2N^x \omega_0\}$ , and the approximation is valid if  $H_e \ll \Delta_0$ . In the opposite limit, i.e.,  $H_e \gg \Delta_0$ , the internal field is close to the external one.

At our particular set of parameters (see the corresponding section) demagnetizing effects at low applied fields play an important role. Therefore in all final equations for the Green functions the external field should be substituted with the internal one. However, in order to keep the notations, we shall use in the following the effective  $\tilde{g}(H_i)$  factor, introduced above, which is a function of the internal but not the external magnetic field. This obstacle seems to be quite essential in view of the nonlinear dependency  $H_i(H_e)$ .

Indeed, conclusions on the behavior of the effective  $\tilde{g}(H_i)$  factor are based on analysis of Eq. (26), in which the external field  $H_e$  should also be substituted with  $H_i$ . As a result, at low fields the  $\tilde{g}(H_e)$  factor does not decrease, as was concluded above, but rather increases with the applied field strength. This is due to the fact that in accordance with Eq. (32) the internal field increases faster than the external

one. The particular behavior  $\tilde{g}$  can in principle be obtained as a result of a numerical solution of Eqs. (26)–(31). It depends not only on the range of applied fields and internal parameters of the system, but also on the shape of a sample. This is, however, beyond of the scope of the present study.

Here we shall not pay anymore attention to this question, mostly for the following reasons. The equations above do not take into account the fluctuational corrections which may play an essential role for a quantitative dependency  $\tilde{g}(H_e)$ . Therefore we shall use  $\tilde{g}$  as a free parameter in the description of our data on inelastic neutron scattering for each value of the magnetic field. Then the field dependencies of  $\tilde{g}$  and other parameters may be analyzed separately, including the analysis of the role in their behavior of the fluctuational corrections. This role is apparently not restricted by only the renormalization of the function  $\tilde{g}(H_e)$ . Rather developed quantum fluctuations should change the behavior of the functions  $\Omega_{1,2q}(H_e)$ . Therefore, in particular, the position of the line given by Eq. (25) may not actually be true, because this equation does not account for the spectrum renormalization.

### G. Fluctuational corrections

Here, with the goal to describe the field dependence of the measured quantities, we restrict ourselves, by the analysis of the general structure of the fluctuational corrections, to the susceptibilities derived above in the MFA. Thus the aims of this analysis are to introduce a proper parametrization of the measured branches of the spectrum, and then to derive the equations, which could be employed in the description of the neutron scattering intensities with the same set of parameters.

The set of parameters of the real Hamiltonian of the system is, actually, not well known, and those found experimentally are already renormalized by the fluctuations, which are quite developed even at low temperatures. Therefore in our preferences in the selection of the diagrams we shall also use the arguments following from the experimental observations. One of the most important among these observations is that the fluctuations do not cause any appreciable damping to the excitations.

Therefore, in the first approximation we should mostly take into account those corrections to the MFA which renormalize, but do not bring broadening into, the spectrum. These kinds of fluctuational corrections arise due to the renormalization of the unit-cell blocks presented in Fig. 1. They correspond to the processes of the self-interaction of a given spin via creation of virtual excitation in the spin medium. Meanwhile, the processes of the interaction of different spins via virtual exchange by the excitations, such as shown in Fig. 1(c), could be in this approximation omitted.

The result of such a renormalization can be summarized in a quite simple way. First, subject to the renormalization is a single-site magnetization  $\mathbf{m}$  and/or the value of the mean effective field. This is reflected in energy shifts of the single-site excitation spectrum and, as discussed above, accounted for by a substitution in the equations for  $\varepsilon_{\lambda\lambda'}$  in Eqs. (9)–(12) with the  $g$  factor for effective  $\tilde{g}(H_i)$  factor, where  $H_i = H_i(H_e)$ .

Then, in the same order of the perturbation expansion, one should renormalize the spin autocorrelation functions

$\Sigma^{\alpha\beta}(\omega)$ . It could be shown that the leading terms in the equations for the corresponding corrections may be accounted for by the introduction of some factors  $Q_x(H_i)$ ,  $Q_y(H_i)$ , and  $Q_z(H_i)$  in a such a manner that  $\Sigma^{xx} \approx Q_x \Sigma_0^{xx}$ ,  $\Sigma^{yy} \approx Q_y \Sigma_0^{yy}$ ,  $\Sigma^{zz} \approx Q_z \Sigma_0^{zz}$ , and  $\Sigma^{yz} \approx Q_{yz} \Sigma_0^{yz}$ , where  $\Sigma_0^{\alpha\beta}$  is given by Eqs. (9)–(12), and  $Q_{yz}^2 = Q_y Q_z$ .

Substituting these expressions into Eqs. (14)–(17), one may calculate the components of the Green function  $G_q^{\mu\nu}(\omega)$  generally represented by Eq. (20). In this equation the frequencies  $\Omega_{1,2q}$  should now be substituted for by the renormalized ones,

$$\tilde{\Omega}_{1q}^2 = \Delta^2 - 2Q_x J_q D^2 / \Delta, \quad (33)$$

$$\tilde{\Omega}_{2q}^2 = \varepsilon_{10}^2 - 2J_q \varepsilon_{10} (\tilde{\Delta} / \Delta) + Q_z Q_y (2\mu H / \Delta)^2 (J_q^2 / \Delta)^2, \quad (34)$$

where  $\tilde{\Delta} = 1/2\{(Q_z + Q_y)\Delta + (Q_z - Q_y)D\}$ . Simultaneously, the amplitudes  $\Lambda^{\mu\nu}$  in Eq. (20) should be substituted for by the following quantities:

$$\tilde{\Lambda}^{xx} = -2Q_x D^2 / \Delta, \quad (35)$$

$$\tilde{\Lambda}^{yy} = -\frac{1}{\Delta} \{2\varepsilon_{10} \tilde{\Delta} - (2\mu H)^2 Q_z [1/2 + Q_y J_q / \Delta]\}, \quad (36)$$

$$\tilde{\Lambda}^{zz} = \frac{1}{\Delta} \{\varepsilon_{10} [Q_y \varepsilon_{10} - \tilde{\Delta}] + 2(\mu H)^2 Q_z Q_y J_q / \Delta\}. \quad (37)$$

The set of Eqs. (33)–(37) completes the parametrization necessary to describe our experimental data. Actually, the parameters  $Q_x$ ,  $Q_y$ ,  $Q_z$ , and  $\tilde{g}$  are functions of the internal magnetic field. Thus  $Q_{xyz}(H_i)$  depends on  $\tilde{g}(H_i)$ , while the latter one is defined by the magnetic susceptibility, which is parametrized by  $Q_{xyz}$ . Therefore, all parameters are correlated and, cannot generally be used in the fitting routine as free. In forthcoming theory they should be expressed via the parameters of the Hamiltonian, which are actual free parameters of the substance. However, since the variation of  $\tilde{g}(H_e)$  and  $Q_{xyz}(H_e)$  with the applied magnetic field is not very pronounced one still may vary them independently.

A complete study would then include a quantitative analysis of the field dependencies of those parameters, and a comparison with the experiment. This, however, invokes some numerical calculations and more accurate measurements, which are both in progress.

### III. EXPERIMENT AND RESULTS

The inelastic neutron-scattering investigations were performed at the cold neutron Three Axis Spectrometer 4F2 at the Laboratoire Léon Brillouin (LLB) at Saclay. All the scans were performed with fixed  $k_f = 1.55 \text{ \AA}^{-1}$  and a beryllium filter in front of the analyzer to suppress higher-order reflections from the analyzer. The collimation was 120', 30', 50', and 50'. The sample of  $\text{RbFeCl}_3$  had a volume of about  $0.4 \text{ cm}^3$ , and the lattice parameters used at low temperature were  $a = 6.991 \text{ \AA}$  and  $c = 5.943 \text{ \AA}$ . The sample temperature was kept at 5.5 K throughout the experiment. This temperature was chosen as a compromise between being far enough above the first phase transformation at 2.55 K and

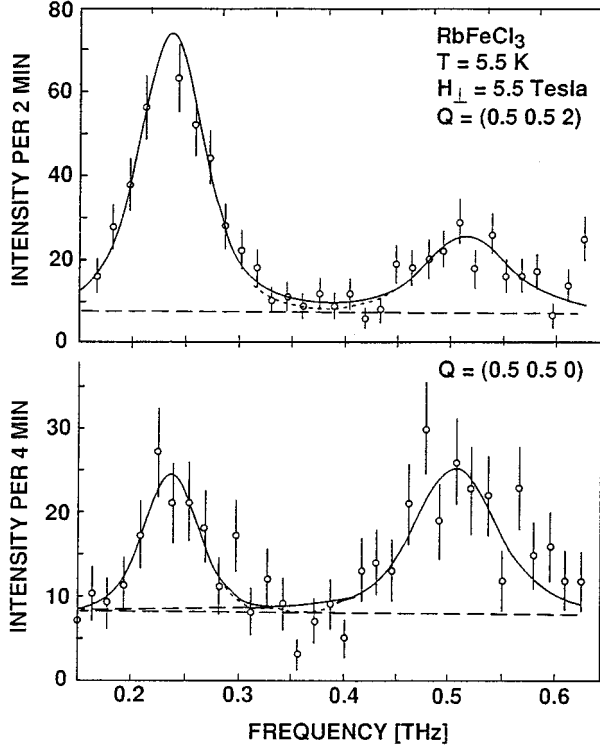


FIG. 2. Constant  $\mathbf{Q}$  scans at the maximum applied field for two equivalent positions in reciprocal space.

being not too high, where damping becomes important. The superconducting magnet of the LLB with vertical field had a maximum field strength of 5.5 T. Data were collected at 0, 2, 3, 4, and 5.5 T.

Two typical experimental scans for the scattering intensities  $I(\mathbf{Q}, \omega)$  measured as functions of the energy transfer  $\omega$  at fixed momentum transfers  $\mathbf{Q}$  are represented in Fig. 2. The scans were performed at the maximum field  $H_{\perp} = 5.5$  T through the modes  $\Omega_1$  and  $\Omega_2$ , the upper and lower frequencies, respectively. The positions  $\mathbf{Q} = (0.5, 0.5, 0)$  and  $\mathbf{Q} = (0.5, 0.5, 2)$  are identical by means of translational symmetry. Similar scans were performed along the  $\mathbf{Q} = (\xi, \xi, l)$  directions for  $l = 0$  and 2.

The data are to be fitted in accordance with the equation

$$I_i(\mathbf{Q}, \omega) = I_0 \int d\omega' R(\mathbf{Q}, \omega - \omega') [N(\omega') + 1] \times (\delta^{\alpha\beta} - e^{\alpha} e^{\beta}) \text{Im} G_{\mathbf{q}}^{\alpha\beta}(\omega', \Omega_{i\mathbf{q}}), \quad (38)$$

where  $R(\mathbf{Q}, \omega - \omega')$  is the resolution function of the spectrometer, and  $\mathbf{e} = \mathbf{Q}/Q$  is a unit vector in the direction of the momentum transfer,  $\mathbf{Q} = \boldsymbol{\tau} + \mathbf{q}$ , where  $\boldsymbol{\tau}$  is a reciprocal-lattice vector. The components of the Green function  $G_{\mathbf{q}}^{\alpha\beta}(\omega', \Omega_{i\mathbf{q}})$  are defined by Eqs. (20) and (33)–(37).

If damping, [i.e., the imaginary part of the self-energy  $\Sigma_{\mathbf{q}}^{\alpha\beta}(\omega)$ ] is ignored, then, in accordance with Eq. (20), one obtains

$$\text{Im} G_{\mathbf{q}}^{\alpha\beta}(\omega) = \frac{\pi \tilde{\Lambda}^{\alpha\beta}}{2\Omega_{i\mathbf{q}}} [\delta(\omega - \Omega_{i\mathbf{q}}) - \delta(\omega + \Omega_{i\mathbf{q}})], \quad (39)$$

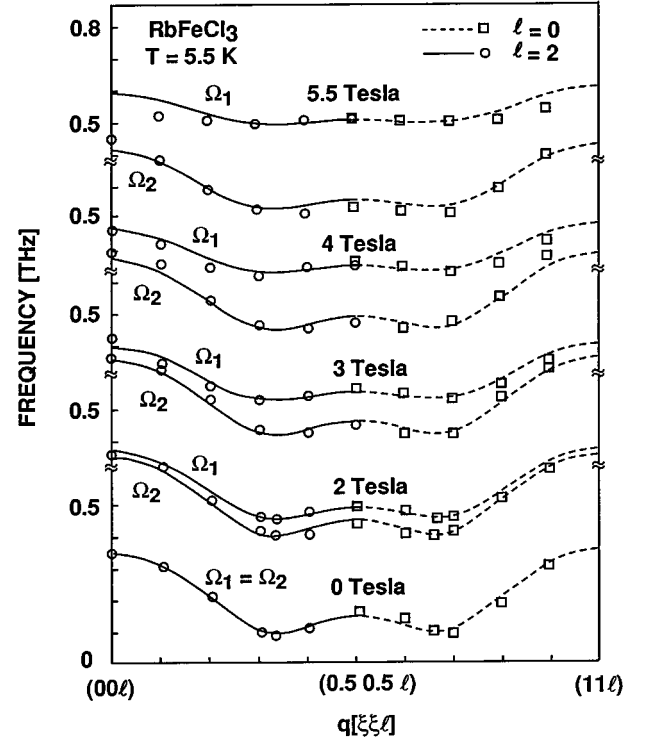


FIG. 3. Dispersion curves of the low-energy magnetic excitations for the direction perpendicular to the chains at different applied fields. The lines represent the best fit of our theory.

and the line shape of the spectra should be entirely described by the resolution function of the instrument. In fact, some small line broadening of the spectra has been detected, and, by means of fitting the data to the damped harmonic-oscillator model, in some cases the intrinsic width came up to 20–50 % of the instrumental resolution. Because the widths of the inelastic scattering peaks were generally small, the resolution was insufficient to arrive at any conclusions about their line shape. For the sake of simplicity, we use Eqs. (38) and (39) for the description of our data. The frequencies of the modes as determined by the fitting routine are presented in Figs. 3–5.

The fitting routine also provided an integrated intensity  $I_{\text{int}}(\mathbf{Q}, \Omega_{i\mathbf{Q}})$  by means of

$$I_{\text{int}}(\mathbf{Q}, \Omega_{i\mathbf{Q}}) = \int d\omega \Omega_{i\mathbf{q}} [N(\omega) + 1]^{-1} I_i(\mathbf{Q}, \omega). \quad (40)$$

From Fig. 2 one can already conclude that the relative intensities of the modes  $\Omega_1$  and  $\Omega_2$  depend strongly on  $\mathbf{Q}$ . A detailed discussion will follow in Sec. IV.

Due to the limited beam time the data are not as complete as one could wish. Nevertheless the statistics were in most cases good enough to determine frequencies. But the precision of determining intensities suffers from large error bars. Mode splitting with increasing field could clearly be observed for the low-frequency modes but at high frequencies near  $l = 1$  the splitting could not be verified within the experimental resolution.

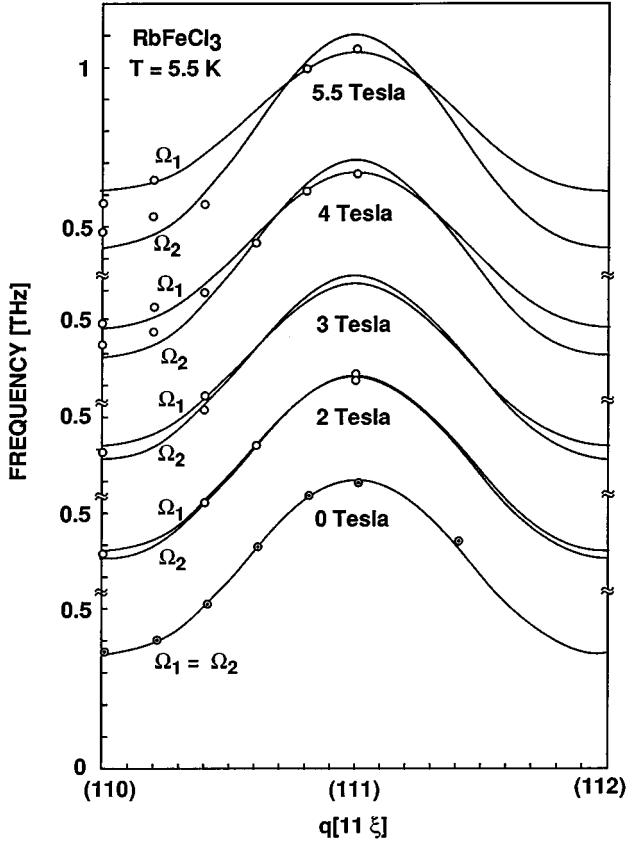


FIG. 4. Dispersion curves of the magnetic excitations along the chain direction for  $(1,1,\xi)$ , which is identical to  $(0,0,\xi)$ . The lines represent the best fit of our theory.

#### IV. DISCUSSION

##### A. Frequencies

The experimentally obtained frequencies were compared to the theoretical predictions. First we fitted the data for the frequencies  $\Omega_1(\mathbf{q})$  and  $\Omega_2(\mathbf{q})$  at zero field to Eqs. (19) and (24) (which coincide for zero field) and obtained the following values of the parameters:

$$D = 0.589 \pm 0.005 [\text{THz}] \approx 19.6 \pm 0.2 [\text{cm}^{-1}],$$

$$J_1 = 0.0743 \pm 0.0007 [\text{cm THz}] \approx 2.48 \pm 0.02 [\text{cm}^{-1}],$$

$$J_2 = -0.0118 \pm 0.0003 [\text{THz}] \approx -0.39 \pm 0.01 [\text{cm}^{-1}],$$

$$J' = -0.0054 \pm 0.0002 [\text{THz}] \approx -0.180 \pm 0.007 [\text{cm}^{-1}].$$

We also repeat for comparison the values for  $\text{CsFeCl}_3$  at 1.6 K (Ref. 13) with  $D = 0.522 \pm 0.003 [\text{THz}]$ ,  $J_1 = 0.0629 \pm 0.0002 [\text{THz}]$ ,  $J_2 = -0.0095 \pm 0.0004 [\text{THz}]$ , and  $J' = -0.0042 \pm 0.0001 [\text{THz}]$ . In accordance with Ref. 5,  $D(\text{RbFeCl}_3) = 0.588 [\text{THz}]$ , and  $D(\text{CsFeCl}_3) = 0.527 [\text{THz}]$ .

As can be seen from Figs. 3–5 the calculated dispersion curves at zero field reproduce the experimental data very well. To calculate the dispersion curves measured under magnetic field we kept these four parameters fixed. Additional parameters, to be varied, were the effective  $\tilde{g}(H_e)$  factor,  $Q_x$ ,  $Q_y$ , and  $Q_z$ ; see Eqs. (33) and (34). The latter ones renormalize the spin autocorrelation functions.

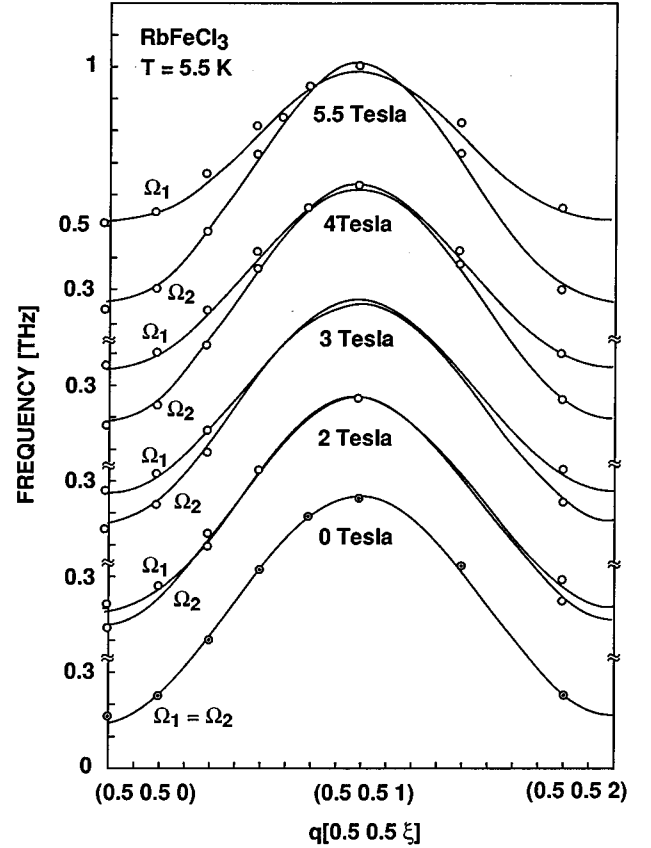


FIG. 5. Dispersion curves of the magnetic excitations along the chain direction for  $(0.5,0.5,\xi)$ . The lines represent the best fit of our theory.

Preliminary fits had shown that the values for  $Q_y$  and  $Q_z$  were nearly the same. Therefore we reduced the number of additional parameters to three setting  $Q_y = Q_z$ .

The values obtained at four different external fields depend on the field, and are shown in Fig. 6. For the parameters  $Q_x$  and  $Q_y = Q_z$ , which by definition have the value 1 at zero field, we interpolated the results by a  $H_\perp^2$  expression as given in Fig. 6. For  $\tilde{g}(H_e)$  this was not possible, because its value at zero field is not known.

Figure 3 shows the low-frequency part of the spectrum, i.e., the dispersion curves perpendicular to the chain direction in the  $[\xi\xi l]$  direction with  $l=0$  and 2. The evolution of the splitting and the shift of the modes is again well reproduced by the theoretical calculations.

In Figs. 4 and 5 we give dispersion curves in the  $[00\xi]$  and  $[0.50.5\xi]$  directions. A splitting could be detected only for  $\xi \leq 0.6$ . This is not surprising, because the theory predicts a mode crossing at about  $l \approx 0.7$ . At wave vectors around this value it is then of course impossible to observe a splitting.

Already in the study of  $\text{CsFeCl}_3$  in an external field perpendicular to the chain axis the results at high frequencies exhibited a discrepancy between experiment and theory. At 6 T and 1.6 K, a splitting could just be observed up to the highest frequencies. However, the theoretical approach<sup>14</sup> used at that time predicted a much larger splitting at high frequencies than observed.

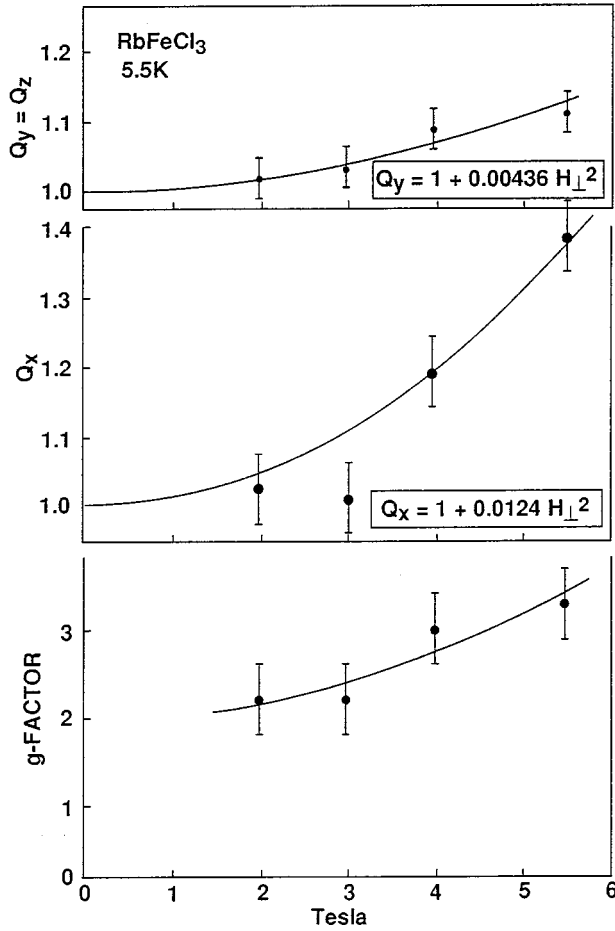


FIG. 6. Field variation of the renormalization parameters  $Q_x(H_\perp)$  and  $Q_y(H_\perp) = Q_z(\perp)$  fitted to quadratic law as given in the inset. For  $\tilde{g}(H_\perp)$ , the line is just a guide to the eye.

### B. Intensities

The determination of intensities in inelastic neutron scattering is a difficult task. Inelastic signals have typically  $10^{-5}$  of the intensities of Bragg reflexes. Therefore spurious effects may easily influence the inelastic intensities. Besides absorption and sample shape, simultaneous Bragg reflections are probably the most dangerous phenomena. While the sample is oriented on a position in an inelastic scan, a Bragg condition may simultaneously be fulfilled for the incoming neutron beam. This reflection takes the intensity out of the primary beam and throws it somewhere into  $4\pi$  space. As a consequence the inelastic signal is reduced.

One way to increase confidence in measured intensities would be to perform the series of experiments at two different neutron energies, as was done<sup>28</sup> before. In the present case we found that intensities at positions near each other in

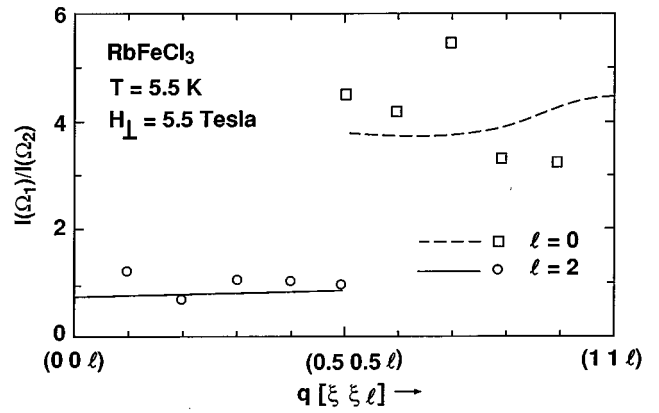


FIG. 7. Intensity ratios of the inelastic scattering signals at the highest applied field from the modes of the two dispersion curves in the direction perpendicular to the chains. The full and dashed lines represent the predictions of our theory.

$\mathbf{Q}$  space could be compared. They could also be followed with increasing field. But there were intensities at a given  $\mathbf{Q}$  which were out of scale in a similar way at all applied fields.

To avoid some of these problems we assumed that both intensities of the split modes are influenced in the same way by spurious effects. This is the reason why we decided to interpret ratios of intensities at the same position in  $\mathbf{Q}$  space. This assumption leaves it still open whether a spurious Bragg reflection comes into play for one of the two signals by means of a variation of the incoming energy during the scan. On the other hand, experience shows that such spurious Bragg reflections were broad with respect to parameters such as incoming energy and sample orientation. The interpretation of ratios also makes unnecessary the estimation of the magnetic form factor and the Debye-Waller factor.

We analyzed the intensities of all scans in  $[\xi, \xi, l]$  directions for  $l=0$  as well as for  $l=2$  using Eq. (40). The ratios  $I_{\text{int}}(\mathbf{Q}, \Omega_1)/I_{\text{int}}(\mathbf{Q}, \Omega_2)$  are presented in Fig. 7 together with the calculated curves. The scatter of the data represents the uncertainties of the experimental results. Nevertheless, it is remarkable how well the calculations reproduce the data. The intensities have been calculated after a fit of the theoretical expressions to the frequencies. Here we want to stress that no further parameters were introduced to calculate intensities. The agreement between experiment and theory is satisfactory, and provides further confidence into the theoretically derived expressions.

### ACKNOWLEDGMENTS

We are greatly indebted to S. V. Maleyev, O. Schärpf, and to M. Steiner for fruitful discussions.

<sup>1</sup>D. Visser and A. Harrison, J. Phys. (Paris) **49**, C8-1467 (1988).

<sup>2</sup>R. Botet, R. Jullien, and M. Kolb, Phys. Rev. B **28**, 3914 (1983).

<sup>3</sup>N. Wada, L. Ubokoshi, and K. Hirakawa, J. Phys. Soc. Jpn. **51**, 2833 (1982).

<sup>4</sup>N. Wada, K. Sumiyoshi, T. Watanabe, and K. Amaya, J. Phys. Soc. Jpn. **52**, 1893 (1983).

<sup>5</sup>H. Yoshizawa, W. Konzukue, and K. Hirakawa, J. Phys. Soc. Jpn. **49**, 144 (1980).

<sup>6</sup>H. Yoshizawa, J. D. Axe, and G. Shirane, Solid State Commun. **38**, 241 (1981).

<sup>7</sup>D. Petitgrand, B. Hennion, P. Radhakrishna, C. Escribe, and S. Legrand, in *Recent Developments in Condensed Matter Physics*,

- edited by J. T. Devreese *et al.* (Plenum, New York, 1981), Vol. 4, p. 205.
- <sup>8</sup>M. Steiner, K. Kakurai, W. Knop, B. Dorner, R. Pynn, U. Happek, P. Day, and G. McLeen, *Solid State Commun.* **38**, 1179 (1981).
- <sup>9</sup>W. Knop, M. Steiner, and P. Day, *J. Magn. Magn. Mater.* **31–34**, 1033 (1981).
- <sup>10</sup>P.-A. Lindgård, *J. Magn. Magn. Mater.* **54–57**, 1227 (1986).
- <sup>11</sup>B. Dorner, D. Visser, and M. Steiner, *Z. Phys. B* **81**, 75 (1990).
- <sup>12</sup>D. Visser, B. Dorner, and M. Steiner, *Physica B* **174**, 25 (1991).
- <sup>13</sup>B. Schmid, B. Dorner, D. Petitgrand, L. P. Regnault, and M. Steiner, *Z. Phys. B* **95**, 13 (1994).
- <sup>14</sup>P.-A. Lindgård and B. Schmid, *Phys. Rev. B* **48**, 13 636 (1993).
- <sup>15</sup>M. Eibschütz, M. E. Lines, and R. C. Sherwood, *Phys. Rev. B* **11**, 4595 (1975); M. E. Lines, *ibid.* **9**, 3927 (1974).
- <sup>16</sup>N. Suzuki, *J. Phys. Soc. Jpn.* **52**, 3907 (1983).
- <sup>17</sup>N. Suzuki, *J. Phys. Soc. Jpn.* **59**, 2947 (1990).
- <sup>18</sup>N. Papanicolaou and P. Spathis, *J. Phys. Condens. Matter* **1**, 5555 (1989).
- <sup>19</sup>V. G. Vaks, A. I. Larkin, and S. A. Pikin, *Zh. Eksp. Teor. Fiz.* **53**, 881 (1967) [*Sov. Phys. JETP* **26**, 188 (1968)].
- <sup>20</sup>V. G. Vaks, A. I. Larkin, and S. A. Pikin, *Zh. Eksp. Teor. Fiz.* **53**, 1089 (1967) [*Sov. Phys. JETP* **26**, 647 (1968)].
- <sup>21</sup>B. P. Toperverg, *Fiz. Tverd Tela (Leningrad)* **14**, 1087 (1978) [*Sov. Phys. Solid State* **14**, 931 (1972)].
- <sup>22</sup>B. P. Toperverg and A. G. Yashenkin, *Phys. Rev. B* **48**, 16 505 (1993).
- <sup>23</sup>T. Tsuboi, M. Chiba, and R. Laiho, *Phys. Status Solidi B* **153**, K159 (1989).
- <sup>24</sup>A. A. Abrikosov, L. P. Gorkov, and I. E. Dzyaloshitski, *Methods of Quantum Field Theory in Statistical Physics* (Prentice-Hall, Englewood Cliffs, NJ, 1963); G. Rickayzen, *Greens Functions and Condensed Matter* (Academic, New York, 1984).
- <sup>25</sup>A. I. Akhiezer, V. G. Ba'ryakhtar, and S. V. Peletminskii, *Spin Waves* (North-Holland, Amsterdam, 1968).
- <sup>26</sup>S. V. Maleev, in *Physics Reviews*, edited by I. M. Khalatnikov (Harwood Academic, Chur, 1987), Vol. 8, Sec. A.
- <sup>27</sup>A. V. Lazuta, S. V. Maleev, and B. P. Toperverg, *Solid State Commun.* **39**, 17 (1981); *Zh. Eksp. Teor. Fiz.* **81**, 2095 (1981) [*Sov. Phys. JETP* **54**, 1113 (1981)].
- <sup>28</sup>H. Boysen, B. Dorner, F. Frey, and H. Grimm, *J. Phys. C* **13**, 1627 (1980).